Micro liquid bridge in periodic electric pulses: The impact of frequency

Miao Sun [1] and Yanbo Xie [2,*]

[1] *School of Aeronautics, Northwestern Polytechnical University, Xi'an 710072, People's Republic of China*

[2] *School of Aeronautics, Institute of Extreme Mechanics and National Key Laboratory of Aircraft Configuration Design, Northwestern Polytechnical University, Xi'an 710072, People's Republic of China*

(Received 4 July 2024; accepted 26 November 2024; published 30 December 2024)

A floating liquid bridge can be generated when voltage is applied across two beakers in DC or high-frequency AC conditions. However, this leaves a wide range of scanning frequencies unknown for the stability of the floating liquid bridge. In this work, we investigated the stability of a micro-floating liquid bridge under periodic voltage pulses, characterized by a high-speed camera and current recording systems. We found that the electrical current perfectly revealed the stability and dynamics of liquid bridges and, thus, can be used as a new approach to study the liquid bridge in the absence of an imaging system. We found six different states of liquid bridges based on their stability, as well as their current characteristics. The phase diagram indicated that, besides the electrocapillary number, the frequency of voltage pulses is another crucial factor for the liquid bridge stability. We unveiled the strong electrical impacts on the liquid bridge formation and breakup dynamics, and we found that the critical time of liquid bridge formation and breakup is an order of magnitude longer than that predicted value, without considering the charging and discharging process. We corrected the formation and breakup time of the floating liquid bridge, considering the Maxwell stress-reduced capillary force in the charging and discharging process, which well explained our experimental observation. Our study provides new insights into the dynamics and stability of liquid bridges, which may be useful for printing in the future.

DOI: 10.1103/PhysRevFluids.9.123701

I. INTRODUCTION

The floating liquid bridge (FLB) was first discovered by Armstrong in 1893 as a free-standing water bridge formed between two beakers when tens of kilovolts were applied [1]. This phenomenon is in the family of electrohydrodynamic phenomena, including Taylor cones and electrospray [2,3], and the latter ones have been widely used in ink-jet printing [4], coating [5], advanced manufacturing [6], and mass spectrum [7]. Although the floating liquid bridge has been known for centuries, the studies were neglected until recent rediscoveries by Fuchs *et al.* [8]. However, enigmas still persist in the studies of floating liquid bridges, both in terms of microscopic water structures and electrohydrodynamics [9–13].

The stability of the floating liquid bridge (FLB) is an important issue. In previous studies, the stable FLB was successfully generated at direct-current (DC) conditions or high frequencies of alternative-current (AC) conditions. Woisetschläger *et al.* successfully generated FLB using polar liquids and high dielectric constants, including water, methanol, ethanol, glycerol, and dimethyl sulfoxide (DMSO) [2,14]. The strong electric field polarized the interface of fluids, causing Maxwell stress to maintain a sustainable interface for the liquid bridge. Nishiumi *et al.* figured out that the

*Contact author: ybxie@nwpu.edu.cn

ions and other factors that disrupt the water dipole arrangement may result in a failure of FLB generation [15]. Taking the floating liquid bridge as an example, the free-standing bridge is capable of forming when the electric field strength exceeds a threshold value, which is in orders of 10^6 V/m [10]. The radius-to-length aspect ratio of the floating liquid bridge (FLB) increases linearly with the rise of electric field strength [16].

A few factors may reduce the floating liquid bridge stability. First, the capillary pressure of the curved free surface may cause pinching and breakup of the liquid bridge. The dynamic process of Newtonian fluid bridge is dominated by the viscosity of liquids and surface forces [17–21]. Burcham *et al.* developed Taylor-Melcher theory that perfectly described the mechanisms of FLB stability that the Maxwell stress of the polarized interface counteracts to the capillary pressure [22]. However, the impacts of the electrified interface on the liquid bridge stability are still under debate. Rubio *et al.* found that the applied voltage may obviously delay the pinching of the free surface, while the polarization stress becomes negligible, and the viscous flow under the action of surface tension dominated the pinch-off process [18].

The gravity is another critical factor for the liquid bridge stability. Montazeri *et al.* proposed that both vertical components of dielectric tension and surface tension hold the bridge against gravity [16]. However, Marín and Lohse discovered interesting results when they noted that increasing voltage amplitude is not always good news for sustaining a stable FLB. When an electric field strength is far beyond the critical electrical strength, the diameter of the liquid bridge increases, resulting in the liquid bridge bearing more gravity force, leading to the collapse or even leakage of FLB when electrical strength decreases [2]. The successful visualization of the water and glycerol mixing demonstrates the high velocity of flows inside the floating liquid bridge [2].

The floating liquid bridge may induce a milliampere level current, which causes a local change of pH values in the beakers, as well as the temperature of liquids by Joule heating. Sammer *et al.* [23] and Woisetschläger *et al.* [24] visualize the flows and pH change in the bridge by using pH dye [23,24]. The electrolysis causes a pH change near the electrodes, which may also generate bubbles. In general, it is interesting that no bubbles were likely observed in the liquid bridge since they possess buoyancy once detached from the electrodes [23]. However, when the bubbles came into the bridge [25] in the outer layer, the local mass density was decreased by the network of bubbles, inducing the instability of the liquid bridge [24].

Fuchs *et al.* [8] and Pan *et al.* [26] characterized the Faraday current-induced temperature rise in the liquid bridge by an Infrared Thermal Imaging Radiometer, and found a surprising rise of temperatures, which causes strong evaporation of liquid and heat dissipation in the complex flows near the beakers [24]. The temperature-raising induced-Joule-heating is proportional to the current amplitude and salt concentration of electrolyte solutions [2,15,26,27], particularly for liquids with high vapor pressure like organic solvents [28]. Qiao *et al.* offered an analytical analysis of jet instability in a thermal field, which may help to understand the liquid bridge break by Joule heating [29]. Fuchs *et al*. provided a thorough understanding from the views of thermodynamics that the temperature rising may disturb the hydrogen bonding and enforce decay of the liquid bridge, leading to the instability of FLB [8].

Woisetschläger *et al.* successfully generated the floating liquid bridges for the first time in an AC situation with the frequencies in order of 1 kHz [24]. In the meantime, Ponterio *et al.* reported the first Raman spectroscopy data on the FLB by alternative voltage with a centimeter-long bridge and found a stable FLB when frequency was above 50 Hz, while lifetime was reduced when frequency was beyond 5 kHz [30]. Their results hardly proved the correlation between liquid bridge formation and microscopic change of water molecular structure. Woisetschläger *et al.* discovered that the critical length of a stable floating liquid bridge becomes shorter when using a high-frequency alternative electric field. Tracer particles were unable to enter the FLB under AC scanning, however, they may penetrate the liquid bridge under directionally applied voltage [14]. Although the stability of FLB has been studied either in DC or high-frequency AC voltage, it still leaves a wide range of frequencies unknown for FLB stability. Ultimately, the impact of an electrified interface on the dynamic processes of FLB formation and breakup is still not clear.

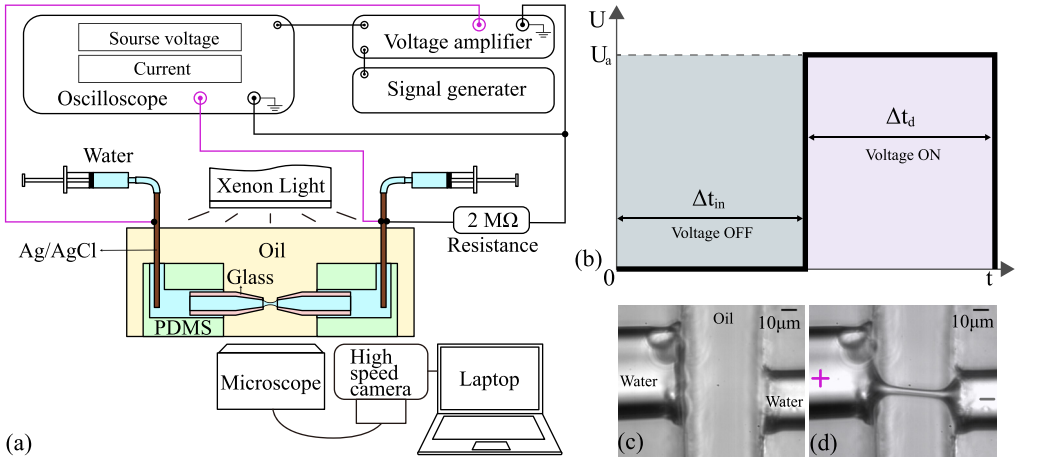

FIG. 1. (a) Experimental setup includes a liquid control system, microscope optical imaging system, and electrical measurement system. (b) Scheme of the square wave of voltage pulses, which is turned ON with time of duration Δt_d and turned OFF with time of pulse interval Δt_{in}. (c) Two opposing micropipettes with liquid-liquid interfaces at initial state. (d) The liquid bridge can form when the appropriate voltage is turned on.

In this work, we investigated the stability of a micro-floating liquid bridge (μFLB) under periodic pulsed voltage in a wide range of frequencies (1 ∼ 100 kHz). We conducted the experiments in an oil bath to avoid water evaporation and plasma and worked with micropipettes to minimize the impact of gravity. With a high-speed camera and electrical measurement system, we could observe the formation and breakup dynamics of the liquid bridge. We found the current recording perfectly represents the identical events of liquid bridge dynamics, in which we identify six phases for the stability of μFLB. Thus, the current recording can be used as a new approach to monitor activities like charging and discharging and the formation of μFLB, even in the absence of a high-speed camera. Our results showed that the charging and discharging of the liquid-liquid (LL) interface plays a significant role in the stability of the μFLB. For instance, the breakup time of the liquid bridge is an order larger than the predicted value by the capillary bridge breakup in previous work, which we attributed to the discharging process at the liquid-liquid interface. We theoretically calculated the formation and breakup time of the liquid bridge, as well as the threshold condition that must incorporate the charging and discharging effects at the LL interface, which well explained the extended breakup time in our experiments. Our work provides a new approach for monitoring the dynamics of liquid bridges by current monitoring, as well as a new understanding of the mechanisms of floating liquid bridge stability.

II. EXPERIMENTAL SET UP

The scheme of the experimental setup is shown in Fig. 1(a). Two opposing glass capillaries with a pipette tip radius of 30 μm and 20 μm were fabricated by a puller (Sutter B100-20-10). These capillaries were then aligned and sealed into a polydimethylsiloxane (PDMS) microfluidic chip connected to two electrodes. The inter-distance between the tips of pipettes was close to 50 μm. The electrolyte solution (1 mM KCl) can be injected via two syringes in the capillaries to control the position of the liquid menisci. The additives of salts can help the current measurement. We also have 1 critical micelle concentration (CMC, 0.05 mM) of nonionic surfactant Tween-20 in the electrolyte solution for the stability of the liquid-liquid interface with reduced surface tension. The microfluidic chip and micropipettes were immersed in a transformer oil bath to prevent water

evaporation and plasma under a strong electric field. The oil has a relative permittivity of 2, a mass density of $0.88\,g/cm^3$, a viscosity of $21\,mPa \cdot s$, and an interfacial tension γ of the water-oil interface of $26\,mN/m$ for later calculations. In our microfluidic system, the Bond number $Bo = \frac{\rho g R_t^2}{\gamma}$ is approximately 3×10^{-4}, thus we could neglect the effects of gravity [31]. As can be seen in Figs. 1(c) and 1(d), there is a bit of size deviation in order of 10 μm between two micropipette tips since the breaking position of the pipette is randomly cut by lasers. In addition, two micropipettes were also slightly mismatched in axial directions, which was caused by a tiny displacement (a few micrometers), of the pipettes (diameter of 20 μm) during the assembly of the devices. However, the small misalignment of micropipettes will not change the μFLB behavior or statistics. Here, we take the effective length of tilted μFLB to determine electric field strength in later calculations.

A high-speed camera (Photon Fastcam WX50) connected with a microscope enables us to observe the formation and breakup processes of the μFLB. We used an arbitrary function generator (Tektronix AFG31021) to produce periodic voltage pulses, which were amplified to hundreds of volts using a voltage amplifier (Aigtek ATA-2161). Two Ag/AgCl electrodes were connected to the micropipettes via PDMS chips for current recordings. A $2\,M\Omega$ resistor was serially connected between the ground terminal of the voltage amplifier and an Ag/AgCl electrode, and parallelly connected to an oscilloscope (TELEDYNE LECROY waverunner 8000) with a $10\,M\Omega$ internal resistance. This setup was used to measure the voltage by dividing the current through the $2\,M\Omega$ resistor for current measurement.

Here, we applied unidirectional square pulse waves in the experiments, with the duration time of each pulse denoted as Δt_d and interval time between pulses denoted as Δt_{in} [Fig. 1(b)]. Thus, we have frequency f of voltage pulses as $f = \frac{1}{(\Delta t_d + \Delta t_{in})}$. Due to the small hydro-pressure from reservoirs, water was likely to fill the tips of glass capillaries, forming a steady water-oil meniscus [Fig. 1(c)]. The applied voltage polarized the LL interface, driving the meniscus of LL interfaces moving toward each other. Once the voltage pulses reached the appropriate amplitude and frequencies, a thin filament of liquid could be formed, as shown in Fig. 1(d). When the voltage was turned off during the interval of two pulses, the liquid bridge may break up and generate a small droplet between two LL interfaces.

III. RESULTS AND DISCUSSION

A. Stability of liquid bridge

We first distinguished six different states according to the stability of μFLB, as well as the measured electric current as functions of voltage amplitude U_a and frequency of voltage pulses f.

First, we set the duration time of the voltage pulse Δt_d equal to the time interval Δt_{in}. Previous work [2] showed the electrocapillary number Ca_e could describe the threshold condition when the liquid bridge has been formed, which is a ratio of Maxwell stress to the capillary pressure of the bridge derived from static force balance. Here, we define the electrocapillary Ca_e in our system as the same form as in the Taylor cone [32–34], which considers the capillary pressure of the meniscus $\sim \frac{\gamma}{R_t}$ before liquid bridge formation, where R_t is the capillary radius:

$$Ca_e = \frac{\varepsilon_0(\varepsilon_w - \varepsilon_s)E^2 R_t}{\gamma}, \tag{1}$$

where ε_0 is the vacuum dielectric constant and ε_w and ε_s are relative dielectric constants of water and surrounding oil, respectively. The electric field strength E is calculated by $\frac{U}{D}$ along the axial direction of the liquid bridge, where D is the distance between two meniscus and R_t is the radius of the pipette.

When $f < 10^4\,Hz$ and $Ca_e < 30$, we didn't observe the formation of a liquid bridge instead of a continuous vibration of the LL interface caused by voltage pulses [I in Fig. 2(a)]. The measured current represents a charging and discharging process with voltage turned on and off, respectively,

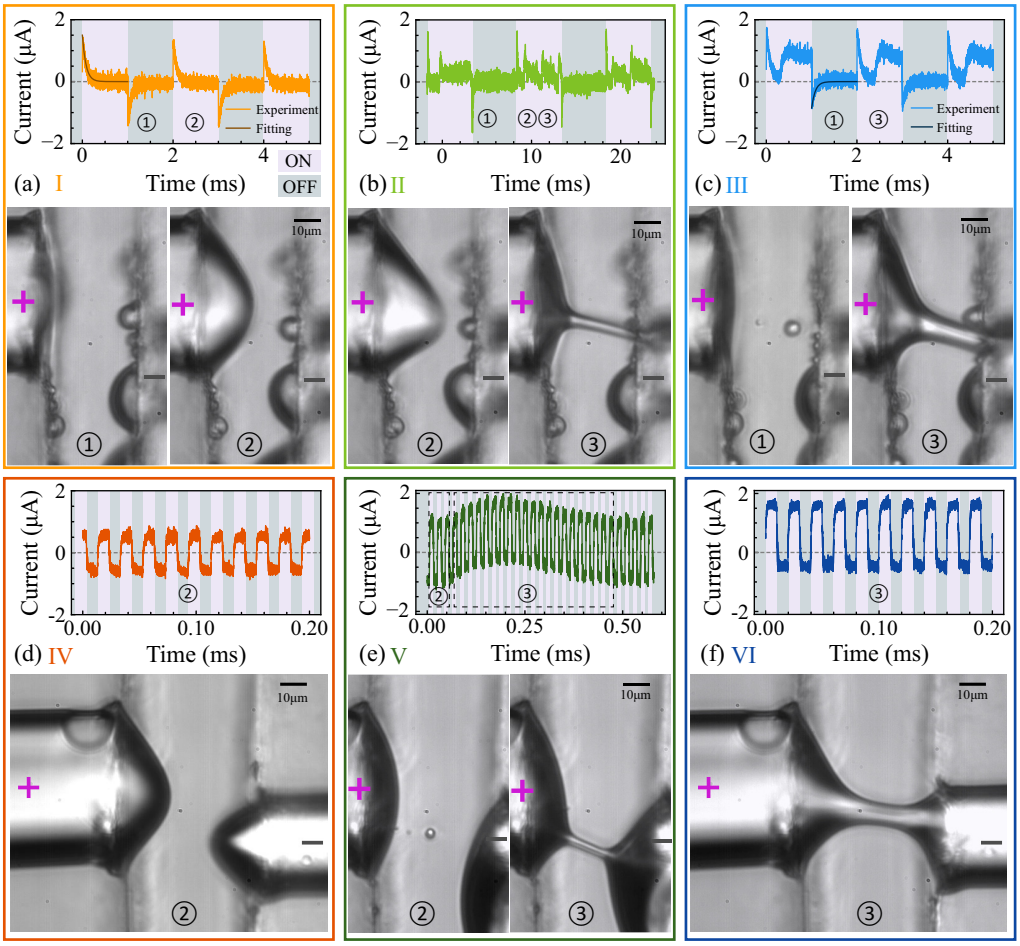

FIG. 2. The distinctive states and corresponding current recording of liquid bridges in periodic voltage pulses. The color and Roman numerals represent different liquid bridge states. The images marked with numbers in a circle correspond to different stages of current annotated on the graphs of current recordings, where ①, ②, ③ indicate the nonpolarized initial state, polarized meniscus, and floating liquid bridge formation. The background color in the current recording shows the regime of voltage being turned on (red) and turned off (grey). (a) The meniscus of the liquid-liquid interface vibrated when $f < 10^4$ Hz (500 Hz) and $Ca_e \ll 30$, with the measured current representing a typical charging and discharging process with a decay time of $\tau_e = 9 \times 10^{-5}$s (brown solid line). (b) The μFLB is capable of forming but is not stable when increasing $Ca_e \sim 30$ at $f < 10^4$ Hz (100 Hz), where current recordings show the μFLB could break at some periods of voltage turned on. (c) The μFLB becomes stable when turning on the voltage when $Ca_e \gg 30$, however, it can break up during voltage pulse intervals when $f < 10^4$ Hz (500 Hz). We increase the electrocapillary number and show the snapshots and corresponding currents in the figures below. (d) The LL interface stabilizes into a Taylor cone configuration under the periodic voltage pulses when $f > 10^4$ Hz (50 kHz) and Ca_e is below 50, with fast charging and discharging current in response to the voltage being turned on and off. (e) The μFLB can form after several pulses at $f > 10^4$ Hz (50 kHz) and $Ca_e \sim 50$, representing a net current after a few pulses. (f) The μFLB becomes stable whenever the voltage is turned on or off when $f > 10^4$ Hz (50 kHz) and $Ca_e \gg 50$, with a net current appearing and vibrating according to the voltage pulses.

due to the capacitance from both the isolated LL interface and the experimental system. According to the charging-discharging curves, we could fit the critical time of charging as $\tau_e = 90\,\mu s$ [brown solid line in Fig. 2(a)].

As we slightly increased the electrocapillary number to about 30 and remained the $f < 10^4$ Hz [II in Fig. 2(b)], we found that a thin liquid filament formed between two glass pipettes. However, this liquid bridge was likely to break while the voltage was still turned on, possibly due to the releasing of charged ions at the capillary interface when two menisci come into contact. The released charges reduce the Maxwell stress, which is insufficient to maintain a stable liquid bridge, causing the μFLB to break again. This results in an accumulation of charges at the menisci, leading to a repeating charging-bridge-break cycle. We observed the cycle by the multiple conduction current spikes formed randomly during one voltage pulse.

As the Ca_e further increased [III in Fig. 2(c)], we found that the liquid bridge became stable when the voltage was applied, but could break up when the voltage was turned off, as marked by the gray regime in Fig. 2(c). When the liquid bridge broke, the liquid interface moved back to the tip of the glass capillaries, leaving a microdroplet at the center. The droplet could be polarized and deformed by the electric field during the next pulse, which will merge with the front of liquid interfaces, forming a new liquid bridge. The electrical current represents nearly all the details of the liquid bridge formation and breakup dynamics. The current represented a typical charging curve when the voltage was turned on. Once the μFLB formed, we could find an obvious conduction current as a constant value above zero. According to the applied voltage and measurement current, the bridge radius R_B matches the conduction relationship $G = \kappa\pi\frac{R_B^2}{L}$ in experiments, where the conductivity of liquids $\kappa = 0.14\,\mathrm{mS/cm}$ and length of liquid bridge $L \approx 25\,\mu m$ here. Once the voltage was turned off, the discharging current appeared, which could not represent the breakup of the liquid bridge. It is still possible to apply a low voltage for the breakup monitoring. However, it may affect the breakup time, as we discussed below. Thus, the current recordings could provide nearly all details of liquid bridge dynamics and could be useful as a new approach for studying liquid bridge stability.

Now we focused on the effects of pulse frequency f. Here, we kept the electrocapillary number of meniscus Ca_e smaller than 50, while gradually increasing f from 1 to 100 kHz. We again observe the vibration of the LL interface without the formation of a liquid bridge when $f > 10\,\mathrm{kHz}$ [IV in Fig. 2(d)]. Since the time intervals Δt_{in} was much smaller than the critical time of discharging τ_e, the meniscus remained stable during the entire experiment, and current rapidly switched between positive and negative values with a mean value close to zero.

As Ca_e increases near the threshold value of 50 at $f > 10\,\mathrm{kHz}$, we found a single pulse is not sufficient enough to charge the LL interface for a liquid bridge [V in Fig. 2(e)]. Instead, several pulses may activate the formation of the liquid bridge, possibly caused by the accumulated charges at the LL interface after several pulses, resulting in the formation of a liquid bridge. Once the liquid bridge was formed, the connection between the two capillaries released the accumulated charges, leading to the breakup of the liquid bridge. It takes another cycle of charge accumulation at the LL interface again, before the liquid bridge formation. A piece of evidence from electrical measurements is that the averaged value of current becomes positive once the liquid bridge is formed, indicating the net transport of ions in the liquid bridge. When we further increased Ca_e above 50 at $f > 10\,\mathrm{kHz}$, we observed a stable liquid bridge whenever the voltage is turned on and off [VI in Fig. 2(f)], representing a constant current via the liquid bridge. The oscillation of current is caused by the periodic voltage pulses.

B. Phase diagrams of liquid bridge

According to the results of high-speed image and electrical measurement, we divide the stability of μFLB into six states as a phase diagram with changes in voltage amplitude and frequency. Each color corresponds to the color of the boxes in Fig. 2. The phase diagram in Fig. 3(a) showed the μFLB is capable of forming at $Ca_e \geqslant 30$ when $f \leqslant 10^4$ Hz. The threshold electrocapillary number

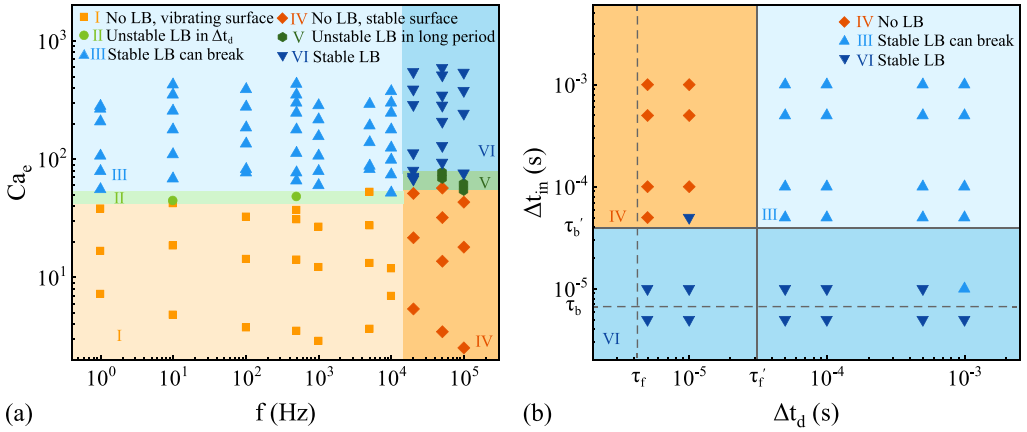

FIG. 3. (a) The phase diagram of the liquid bridge stability as functions of voltage pulse frequency and electrocapillary number, when $\Delta t_{\mathrm{d}} = \Delta t_{\mathrm{in}}$. The color and Roman numerals correspond to the identical phase in Fig. 2. (b) A phase diagram of liquid bridge stability as functions of time duration Δt_{d} and time intervals Δt_{in} of voltage pulses with a constant electrocapillary number $Ca_{\mathrm{e}} = 130$. The color and phases also correspond to the identical phase in Fig. 2.

Ca_{e} increased a bit at high frequencies, which is possibly caused by the unsaturated charging process at the liquid meniscus during the Δt_{in}. However, the large Ca_{e} is not the only factor for a stable liquid bridge, as we found unsteady μFLB in a low frequency. As seen in the phase diagram, we found the μFLB will become stable only when the threshold f is over $\sim 10^4$ Hz, which indicates the time duration Δt_{d} and interval Δt_{in} of pulses play a role for the stability of the liquid bridge.

Thus, we investigated the stability of μFLB as a function of the time duration of the pulse Δt_{d} and time intervals Δt_{in} of the pulse, as shown in Fig. 3(b), which correlated to the formation and breakup dynamics of μFLB. Here we set $Ca_{\mathrm{e}} \approx 130$ to ensure the Maxwell stress is strong enough to form a μFLB, meanwhile adjust the Δt_{d} and Δt_{in} of voltage pulses to study the liquid bridge stability. We found a regime that the μFLB is not capable if forming in such a high Ca_e number when $\Delta t_{\mathrm{d}} < 20\,\mu\mathrm{s}$ and $\Delta t_{\mathrm{in}} > 20\mu\mathrm{s}$. The menisci of the LL interfaces slightly move forward and even stay at the initial position when $\Delta t_{\mathrm{d}} \ll \Delta t_{\mathrm{in}}$, corresponding to the phase IV. The dynamics of liquid bridge breakup need to be considered. When $\Delta t_{\mathrm{in}} < 20\,\mu\mathrm{s}$, we found a stable μFLB as phase VI marked in dark blue. While the μFLB could keep stable during pulse duration but break at pulse interval once $\Delta t_{\mathrm{d}} > 20\,\mu\mathrm{s}$ and $\Delta t_{\mathrm{in}} > 20\,\mu\mathrm{s}$ as phase III marked in light blue in Fig. 3(b). Our results indicate that the electrocapillary number, derived from static mechanics, is not capable of describing the stability of μFLB in periodic pulses. Thus, we will discuss the impacts of Δt_{in} and Δt_{d} in the following texts.

C. Liquid bridge formation

Maxwell stress drives the liquid-liquid interface of two menisci from capillaries moving toward each other and may eventually contact. Assuming the liquid menisci from two capillaries under a certain electric field strength E with the pulse duration time t_{d} and displacement of $\sim\frac{D}{2}$. We can derive the acceleration of the meniscus front by Newton's law $a \sim \frac{\varepsilon_0(\varepsilon_{\mathrm{w}}-\varepsilon_{\mathrm{s}})E^2}{2\rho R_{\mathrm{t}}}$, when located at z position and time t. Thus, the mean acceleration over the entire trajectory prior to displacement of z is given by $\bar{a} \sim \frac{1}{z}\int a(z)\mathrm{d}z$, where the electric field strength is expressed as $E = \frac{U_{\mathrm{a}}}{D}$. ρ, R_{t}, D are water mass density, capillary tip radius, and the distance of the two menisci at initial condition, respectively. Two menisci moved forward by a distance of $\frac{D}{2} \sim \frac{1}{2}\bar{a}\tau_{\mathrm{f}}^2$ with the mean acceleration

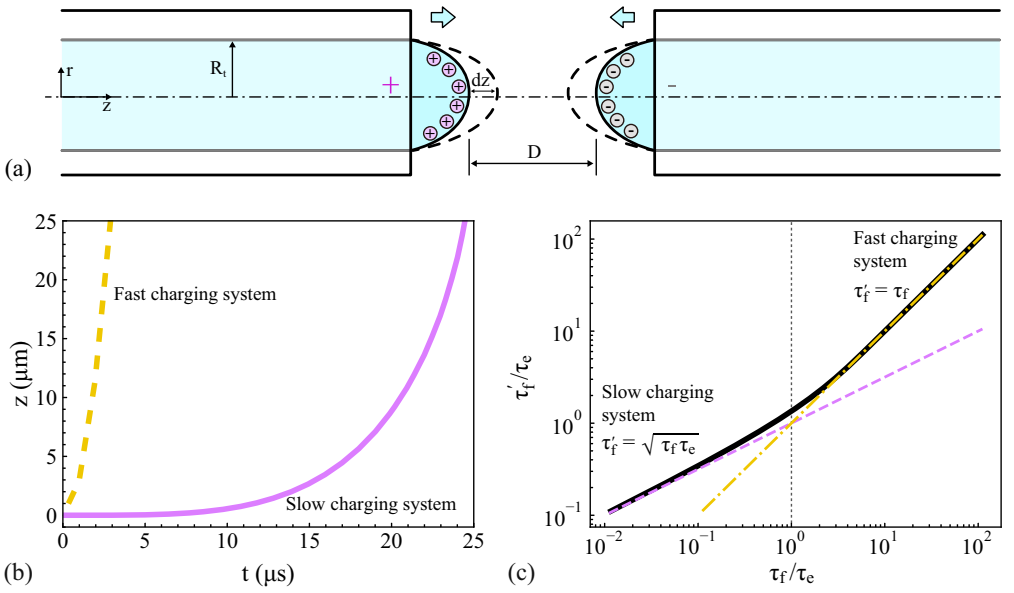

FIG. 4. (a) A scheme of liquid bridge formation process. (b) The displacement z of the menisci front during the formation process. The motion of the liquid-liquid interface at a fast charging system (yellow dashed line) apparently moves faster than the slow-charging system (purple solid line). (c) The corrected time of the liquid front connection (black solid line) can be approximated as $\sqrt{\tau_f \tau_e}$ at a slow charging system, however equals to τ_f at a fast charging system.

calculated by $\bar{a} \sim (\frac{2}{D}) \int_0^{\frac{D}{2}} a(z)\mathrm{d}z$. Thus, we could derive the time of liquid surface contact under a stable electric field as follows:

$$\tau_f \sim \frac{1}{E}\sqrt{\frac{D\rho R_t}{\varepsilon_0(\varepsilon_w - \varepsilon_s)}}. \tag{2}$$

However, the τ_f shown as a dashed line in Fig. 3(b) is an order smaller to define the boundary of the stability phases. We suspect the charging process may play a role in the formation process of the μFLB, since the system resistance significantly increased in the microfluidic system compared to the beaker system, where the charges could be stored at the liquid-liquid interface, behaving as a capacitance. We derived the critical time of the charging process by fitting the current in Fig. 2(a), thus we replaced the electric field as $E(t) = \frac{U_a}{D-2z}(1 - e^{-\frac{t}{\tau_e}})$. Considering the charging process of the liquid interface, we replaced the constant electric field strength in the acceleration a with the time-dependent electric field strength $E(t)$, and derived the motion equation $\frac{D}{2} \sim \frac{1}{2}\bar{a}\tau_f^2$. We can approximate the formation time τ_f' of a liquid bridge considering the charging process, which could be corrected by τ_f as the following expression:

$$\tau_f'\left(1 - e^{-\frac{\tau_f'}{\tau_e}}\right) = \tau_f. \tag{3}$$

We could calculate Eq. (3) shown as the black solid line in Fig. 4(c), which shows a clear transition of the liquid bridge formation time. In a fast charging system $\tau_f \gg \tau_e$, the time of liquid bridge formation equals to τ_f in Eq. (2), as described in the previous beaker system. However, when it comes to a slow charging system $\tau_f \ll \tau_e$, the time of liquid bridge formation can be approximated as $\sqrt{\tau_f \tau_e}$. The calculated value τ_f' in our system is about 24 μs, which well defines the boundary of the phase diagram in Fig. 3(b) and is consistent with our experimental observation. According to

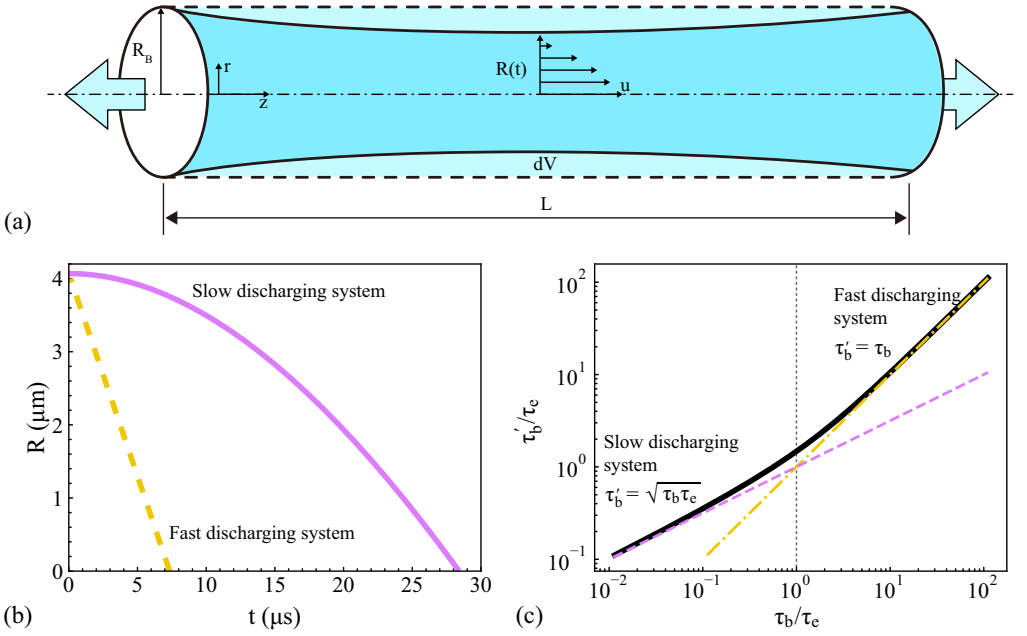

FIG. 5. (a) A scheme of liquid bridge breakup process. (b) The radius of the liquid bridge decreases as time passes, where a fast discharging system (yellow) breaks faster than a slow discharging system (purple). (c) The breakup time of a liquid bridge, which equates to a neutral capillary bridge τ_b in a fast discharging system, will become $\sqrt{\tau_b \tau_e}$ in a slow discharging system.

Eq. (2), for the floating liquid bridge in the beaker system, it comes to a fast charging regime $\frac{\tau_b}{\tau_e} > 1$. As a consequence, the charging time can be ignored in the formation of the FLB in beakers [26].

D. Liquid bridge breakup

The breakup time of liquid bridges is critical for their stability. The breakup time of the floating bridge was estimated by using polarized-free capillary bridge breakup [17,18]

$$\tau = \frac{14.1 \eta R_B}{\gamma}, \tag{4}$$

where η is the viscosity of water and $R_B \sim 4\,\mu m$ is the radius of the liquid bridge, and the constant factor is derived from the similar solution of Stokes flow [19]. We derived a theoretical value of the breakup time τ_f of 7 μs from Eq. (4), an order smaller than the value of τ_f' defining the boundary of the phase III and IV in the phase diagram [Fig. 3(b)]. We suspect the extended breakup time was caused by the slow discharging process at the intervals of voltage pulses.

Here we consider the breakup process as the volume flow out of the cylinder in a viscous system [Fig. 5(a)]. The capillary pressure of the curved LL interface squeezes the cylinder and drives the volume flow out of the bridge [35], ignoring the pinch-off time of the extremely fine filament at the end of the breakup process [36]. In our axisymmetric microbridge, the Reynolds number is less than 1, and the net flow in the radial direction is far smaller than that at the axial direction, which is comparable to the free flows in the confinement system [37,38]. As a result, the axial pressure gradient is provided by capillary force $\frac{\partial p}{\partial z} \sim \frac{\gamma}{LR_B}$. Thus, we have the flow rate $Q \sim \frac{\gamma}{8\eta L}\pi R^3(t)$ equals to the volume change per unit time $\frac{dV}{dt} = \frac{\pi L(R^2-(R-dR)^2)}{dt} \sim 2\pi LR\frac{dR}{dt}$. Thus, we have the radius

change as a function of time as follows:

$$\frac{\mathrm{d}R}{\mathrm{d}t} \sim \frac{\gamma R^2}{16\eta L^2}. \tag{5}$$

If we approximate the length L to be of the same order as the liquid bridge radius R_B, and use a first-order approximation $\mathrm{d}R/\mathrm{d}t \sim R_\mathrm{B}/\tau_\mathrm{b}$. We have similar equations for the charge-free capillary breakup time, as seen in Eq. (4) and previous work [17,35],

$$\tau_\mathrm{b} \sim \frac{16\eta R_\mathrm{B}}{\gamma}. \tag{6}$$

When we consider an electrified liquid-liquid interface, which still bears a residual Maxwell stress at intervals of the voltage pulses, the effective surface tension can be considered as $\gamma = \gamma_0 - \varepsilon_0(\varepsilon_\mathrm{w} - \varepsilon_\mathrm{s})E^2(t)R_\mathrm{B}$ [39,40]. The discharge process during the breakup is symmetrical to the charging process during formation, thus the residual electric field can be expressed as $E(t) = E_\mathrm{m} \cdot e^{-\frac{t}{\tau_\mathrm{e}}}$, where E_m is the electric field strength of a fully polarized interface under applied voltage $E_\mathrm{m} = \frac{U_\mathrm{a}}{L}$. Thus, we have the corrected surface tension as $\gamma = \gamma_0(1 - Ca'_\mathrm{e})$, where the Ca'_e is the electrocapillary number of a liquid bridge expressed as $Ca'_\mathrm{e} = \frac{\varepsilon_0(\varepsilon_\mathrm{w}-\varepsilon_\mathrm{s})E^2(t)R_\mathrm{B}}{\gamma_0}$. Since the electrified LL interface is balanced between the capillary force and Maxwell stress, it indicates the $Ca'_\mathrm{e}(t=0) = 1$ at the initial state of a breakup process. Thus, the time-dependent electrocapillary number Ca'_e can be approximated as $Ca'_\mathrm{e} = e^{-\frac{2t}{\tau_\mathrm{e}}}$ during the discharging process. Replacing the surface tension with consideration of the discharging process in Eq. (5), we have a corrected breakup time τ'_b as functions of τ_b and τ_e, expressed as follows:

$$\tfrac{1}{2}\tau_\mathrm{e}\left(e^{-\frac{2\tau'_\mathrm{b}}{\tau_\mathrm{e}}} - 1\right) + \tau'_\mathrm{b} = \tau_\mathrm{b}. \tag{7}$$

Taking the values of $\eta = 3\,\mathrm{mPa}\cdot\mathrm{s}$, $R_\mathrm{B} = 4\,\mu\mathrm{m}$, $\gamma = 26\,\mathrm{mN/m}$, and $\tau_\mathrm{e} = 90\,\mu\mathrm{s}$, we have the corrected breakup time of μFLB, $\tau'_b = 27\,\mu\mathrm{s}$, well predicting the boundary of phase III and VI of our experimental results, shown in Fig. 3(b), where the time of polarized-free capillary breakup [Eq. (6)] failed. It needs to be noted, that our current theory is applicable to the thinning dynamics of liquid bridge filaments, which is possibly different from the pinch-off process with a droplet formation.

It is interesting to note, that the μFLB remains stable once the formation time is smaller than the pulse duration $\Delta t_\mathrm{d} < \tau'_\mathrm{f}$. It could be understood that the time of liquid bridge formation is shorter than the time of meniscus receding after breakup, which always induces the meniscus to move toward each other until connected. The time of meniscus receding could be estimated by $\tau_\mathrm{r} = \sqrt{\frac{L\rho R_\mathrm{t}}{\gamma}}$ [41] under the action of capillary pressure from the menisci of liquid-liquid surfaces. When the electrocapillary number reaches 30, the Maxwell stress is an order higher than the capillary pressure, and the meniscus acceding is faster than their receding $\tau_\mathrm{r} < \tau_\mathrm{f}$, thus causing a liquid bridge formation. The critical time of liquid bridge generation and breakup are in order of magnitude of 10^{-5} s, which is apparently smaller than the 50 ms previously reported [30]. Such deviation of frequency can be attributed to two factors. First, the diameter of the liquid bridge in our system is three orders of magnitude smaller than the beaker system, which significantly reduces the breakup time in our system. Second, in previous studies, the polarization of the LL interface by a sinusoidal voltage [24,30] may differ from our system. We used a series of square positive waves that continuously charged the interface, thereby reducing the formation and breakage time of the liquid bridge. Although our results showed that a charging and discharging process may change the stability of the micro-floating liquid bridge, there are still mysteries of the μFLB, particularly on the molecular scale. Recently, Wexler *et al.* studied the water behavior by Raman spectroscopy, whose results suggest a transition of the water phase from a long-range disordered state to dipole-dipole interactions under high voltage [42,43], which possibly provides deep understanding at molecular views.

Our results indicate that working with the micro liquid bridge in an oil bath has a few advantages, such as minimizing the voltage amplitude, Joule heating, electrolysis-produced bubbles, negligible gravity impacts, and evaporation of water. However, it also brings some challenges with optical imaging, as the formation and breakup dynamics become much faster than in the beaker system. We are confident that the current findings indicate the impact of voltage pulse frequency is critical for the FLB stability, as well as the electrocapillary number. Additionally, the phase diagram of FLB stability and threshold conditions of charging and discharging governed FLB, could be helpful in the understanding of debated results on liquid bridge formation and breakup dynamics.

IV. CONCLUSION

In this work, we studied the stability of a micro-floating liquid bridge by using periodic voltage pulses. We operated the experiments in an oil bath, avoiding the evaporation of water. The benefits of working with micro liquid bridge include minimizing the voltage amplitude, thereby reducing the generation of bubbles and Joule heating that enhances evaporation, as well as avoiding the impacts of gravity.

We found the six states of the liquid bridge characterized by both the high-speed camera in the microscope and the current recordings, which are determined by wave functions and amplitude of voltage pulses, as drawn in a phase diagram. The liquid bridge dynamics, such as the charging and discharging and formation processes, can be excellently identified by the current recordings, thus, the current recordings can be useful for the monitoring of liquid bridge stability. We found the electrocapillary number is not the only factor that determined the stability of the liquid bridge, but also the frequency of electric pulses. The threshold electrocapillary number for the generation of the micro-floating liquid bridge is approximately 30 at frequencies lower than 10^4 Hz and approximately 50 at frequencies higher than 10^4 Hz. However, the micro-floating liquid bridge becomes stable when the time intervals of voltage pulses become less than 27 μs.

Our experimental results from the phase diagram show that the charge effects at the interface play an important role. We developed the critical time of micro floating liquid bridge formation using a correction factor considering the polarized interface, which is determined by the charging process of the liquid meniscus in our micro liquid bridge system, as well as the motion of the LL interface. Meanwhile, the breakup time of the liquid bridge is an order higher than predicted by charge-free capillary bridge breakup, which we attributed to the slow discharging process in the micro liquid bridge where the charges reduced the capillary force, thus slowing down the breakup process as also recently discovered by Farrokhi *et al.* [40]. Thus, we give a breakup time of a micro-floating liquid bridge considering the charged interface, which well describes our experimental results.

Our work proposes that the current recordings can be a useful tool for measuring the liquid bridge stability, and the polarized interface could be a significant factor in the formation and breakup dynamics of the liquid bridge. The underlying physics of corrected liquid bridge dynamics could be useful for the correlated electrohydrodynamic phenomena and their applications.

ACKNOWLEDGMENTS

The authors would like to acknowledge Dr. Xurui Zhang from the School of Aerospace Engineering in Xi'an Jiaotong University for the help with glass pipettes, Dr. Guoliang Chen from Max-ray Photonics Technology Co., Ltd., and Dr. Jiwei Zhang from the School of Physical Science and Technology in Northwestern Polytechnical University for the help with the optical imaging system, and Professor Hengdong Xi from the School of Aeronautics in Northwestern Polytechnical University for useful discussion. This work was supported by the National Natural Science Foundation of China Grants No. 12075191, No. 12388101, No. 12241201, and the Fundamental Research Funds for the Central Universities with Grant No. D5000210626.

[1] W. Armstrong, Electrical phenomena the newcastle literary and philosophical society, Electr. Eng. **10**, 153 (1893).
[2] Á. G. Marín and D. Lohse, Building water bridges in air: Electrohydrodynamics of the floating water bridge, Phys. Fluids **22**, 122104 (2010).
[3] G. Riboux, A. G. Marín, I. G. Loscertales, and A. Barrero, Whipping instability characterization of an electrified visco-capillary jet, J. Fluid Mech. **671**, 226 (2011).
[4] K. H. Choi, A. Khan, H.-C. Kim, K. Rahman, K. R. Kwon, N. M. Muhammad, and Y. H. Doh, Electrohydrodynamic Inkjet-micro pattern fabrication for printed electronics applications, in *Recent Advances in Nanofabrication Techniques and Applications*, edited by B. Cui (InTech, Rijeka, Croatia, 2011).
[5] C. Guo, J. Zhou, Y. Chen, H. Zhuang, J. Li, J. Huang, Y. Zhang, Y. Chen, S. L. Li, and Y. Q. Lan, Integrated micro space electrostatic field in aqueous zn-ion battery: Scalable electrospray fabrication of porous crystalline anode coating, Angew. Chem. Int. Edit. **135**, e202300125 (2023).
[6] L. Liu, X. Yan, L. Li, J. Su, S. Ramakrishna, Y. Z. Long, and W. Han, Preparation of high-performance graphene materials by adjusting internal micro-channels using a combined electrospray/electrospinning technique, J. Alloy. Compd. **940**, 168882 (2023).
[7] G. R. D. Prabhu, E. R. Williams, M. Wilm, and P. L. Urban, Mass spectrometry using electrospray ionization, Nat. Rev. Method. Prime. **3**, 23 (2023).
[8] E. C. Fuchs, J. Woisetschläger, K. Gatterer, E. Maier, R. Pecnik, G. Holler, and H. Eisenkölbl, The floating water bridge, J. Phys. D: Appl. Phys. **40**, 6112 (2007).
[9] L. B. Skinner, C. J. Benmore, B. Shyam, J. K. R. Weber, and J. B. Parise, Structure of the floating water bridge and water in an electric field, Proc. Natl. Acad. Sci. USA **109**, 16463 (2012).
[10] O. Teschke, D. Mendez Soares, and J. F. Valente Filho, Floating liquid bridge tensile behavior: Electric-field-induced young's modulus measurements, Appl. Phys. Lett. **103**, 251608 (2013).
[11] L. Piatkowski, A. D. Wexler, E. C. Fuchs, H. Schoenmaker, and H. J. Bakker, Ultrafast vibrational energy relaxation of the water bridge, Phys. Chem. Chem. Phys. **14**, 6160 (2012).
[12] E. C. Fuchs, A. Cherukupally, A. H. Paulitsch-Fuchs, L. L. F. Agostinho, A. D. Wexler, J. Woisetschläger, and F. T. Freund, Investigation of the mid-infrared emission of a floating water bridge, J. Phys. D: Appl. Phys. **45**, 475401 (2012).
[13] G. M. Kontogeorgis, A. Holster, N. Kottaki, E. Tsochantaris, F. Topsøe, J. Poulsen, M. Bache, X. Liang, N. S. Blom, and J. Kronholm, Water structure, properties and some applications – a review, Chem. Thermodynamics and Therm. Anal. **6**, 100053 (2022).
[14] J. Woisetschläger, A. D. Wexler, G. Holler, M. Eisenhut, K. Gatterer, and E. C. Fuchs, Horizontal bridges in polar dielectric liquids, Exp. Fluids **52**, 193 (2012).
[15] H. Nishiumi and F. Honda, Effects of electrolyte on floating water bridge, Adv. Phys. Chem. **2009**, 371650 (2009).
[16] R. Montazeri Namin, S. Azizpour Lindi, A. Amjadi, N. Jafari, and P. Irajizad, Experimental investigation of the stability of the floating water bridge, Phys. Rev. E **88**, 033019 (2013).
[17] G. H. McKinley, Visco-elasto-capillary thinning and break-up of complex fluids, Annu. Rheo. Rev. **15**, 12 (2005).
[18] M. Rubio, A. Ponce-Torres, M. A. Herrada, A. M. Gañán-Calvo, and J. M. Montanero, Effect of an axial electric field on the breakup of a leaky-dielectric liquid filament, Phys. Fluids **33**, 092114 (2021).
[19] D. T. Papageorgiou, On the breakup of viscous liquid threads, Phys. Fluids **7**, 1529 (1995).
[20] L. Yang, Y. Tu, and H. Fang, Modeling the rupture of a capillary liquid bridge between a sphere and plane, Soft Matter **6**, 6178 (2010).
[21] F. Yang and Y.-P. Zhao, The effect of a capillary bridge on the crack opening of a penny crack, Soft Matter **12**, 1586 (2016).
[22] C. L. Burcham and D. A. Saville, Electrohydrodynamic stability: Taylor–Melcher theory for a liquid bridge suspended in a dielectric gas, J. Fluid Mech. **452**, 163 (2002).
[23] M. Sammer, A. D. Wexler, P. Kuntke, H. Wiltsche, N. Stanulewicz, E. Lankmayr, J. Woisetschläger, and E. C. Fuchs, Proton production, neutralisation and reduction in a floating water bridge, J. Phys. D: Appl. Phys. **48**, 415501 (2015).

[24] J. Woisetschläger, K. Gatterer, and E. C. Fuchs, Experiments in a floating water bridge, Exp. Fluids **48**, 121 (2010).
[25] E. C. Fuchs, K. Gatterer, G. Holler, and J. Woisetschläger, Dynamics of the floating water bridge, J. Phys. D: Appl. Phys. **41**, 185502 (2008).
[26] X. Pan, M. Hu, B. Xu, F. Wang, P. Huo, F. Chen, Z. Gu, and D. Deng, Armstrong liquid bridge: Formation, evolution and breakup, Phys. Rev. Fluids **6**, 093901 (2021).
[27] A. D. Wexler, M. L. Sáenz, O. Schreer, J. Woisetschläger, and E. C. Fuchs, The preparation of electrohydrodynamic bridges from polar dielectric liquids, J. Vis. Exp. **91**, e51819 (2014).
[28] E. C. Fuchs, A. D. Wexler, L. L. F. Agostinho, M. Ramek, and J. Woisetschläger, Methanol, ethanol and propanol in EHD liquid bridging, J. Phys.: Conf. Ser. **329**, 012003 (2011).
[29] R. Qiao, K. Mu, and T. Si, Analytical instability theory of a liquid jet under a thermal field, Acta Mech. Sin. **39**, 323086 (2023).
[30] R. C. Ponterio, M. Pochylski, F. Aliotta, C. Vasi, M. E. Fontanella, and F. Saija, Raman scattering measurements on a floating water bridge, J. Phys. D: Appl. Phys. **43**, 175405 (2010).
[31] M. A. Herrada, J. M. López-Herrera, A. M. Gañán Calvo, E. J. Vega, J. M. Montanero, and S. Popinet, Numerical simulation of electrospray in the cone-jet mode, Phys. Rev. E **86**, 026305 (2012).
[32] A. Yazdekhasti, A. Pishevar, and A. Valipouri, Investigating the effect of electrical conductivity on electrospray modes, Exp. Therm. Fluid Sci. **100**, 328 (2019).
[33] J. C. Baygents, N. J. Rivette, and H. A. Stone, Electrohydrodynamic deformation and interaction of drop pairs, J. Fluid Mech. **368**, 359 (1998).
[34] J. C. Bird, W. D. Ristenpart, A. Belmonte, and H. A. Stone, Critical angle for electrically driven coalescence of two conical droplets, Phys. Rev. Lett. **103**, 164502 (2009).
[35] V. Entov and E. Hinch, Effect of a spectrum of relaxation times on the capillary thinning of a filament of elastic liquid, J. Non-Newtonian Fluid Mech. **72**, 31 (1997).
[36] Y. Li and J. E. Sprittles, Capillary breakup of a liquid bridge: Identifying regimes and transitions, J. Fluid Mech. **797**, 29 (2016).
[37] U. P. Singh, R. S. Gupta, and V. K. Kapur, On the steady performance of hydrostatic thrust bearing: Rabinowitsch fluid model, Tribol. Trans. **54**, 723 (2011).
[38] J.-R. Lin, Non-newtonian effects on the dynamic characteristics of one-dimensional slider bearings: Rabinowitsch fluid model, Tribol. Lett. **10**, 237 (2001).
[39] J. Melcher and E. Warren, Electrohydrodynamics of a current-carrying semi-insulating jet, J. Fluid Mech. **47**, 127 (1971).
[40] S. J. Farrokhi, A. D. Ratschow, and S. Hardt, Electrostatics slows down the breakup of liquid bridges on solid surfaces, arXiv:2410.17679.
[41] F. Li, S.-Y. Ke, X.-Y. Yin, and X.-Z. Yin, Effect of finite conductivity on the nonlinear behaviour of an electrically charged viscoelastic liquid jet, J. Fluid Mech. **874**, 5 (2019).
[42] A. D. Wexler, E. C. Fuchs, J. Woisetschläger, and G. Vitiello, Electrically induced liquid–liquid phase transition in water at room temperature, Phys. Chem. Chem. Phys. **21**, 18541 (2019).
[43] A. D. Wexler, S. Drusová, J. Woisetschläger, and E. C. Fuchs, Non-equilibrium thermodynamics and collective vibrational modes of liquid water in an inhomogeneous electric field, Phys. Chem. Chem. Phys. **18**, 16281 (2016).